Nano Research

Open Access

Research Article

Amino acid assisted aqueous synthesis of highly stable $CsPbBr_3$ nanocrystals for cell imaging

Xue Li[1], Yanan Guo[1], Guoying Tan[1], Qingyi Liu[1], Nan Song[1] ✉, and Yu Tang[1,2] ✉

[1] *State Key Laboratory of Applied Organic Chemistry, Key Laboratory of Nonferrous Metal Chemistry and Resources Utilization of Gansu Province, College of Chemistry and Chemical Engineering, Lanzhou University, Lanzhou 730000, China*
[2] *State Key Laboratory of Baiyunobo Rare Earth Resource Researches and Comprehensive Utilization, Baotou Research Institute of Rare Earths, Baotou 014030, China*

Cite this article: *Nano Research*, **2025**, *18*, 94907067. https://doi.org/10.26599/NR.2025.94907067

ABSTRACT: Lead halide perovskite nanocrystals (NCs) exhibit excellent optoelectronic performance and have drawn great interests in the fields of biological imaging and sensing. However, the poor stability of $CsPbX_3$ (X = Cl, Br, I) in water is still a challenge to hinder their practical applications. In this work, a facile strategy has been developed for aqueous synthesis of $CsPbX_3$ nanocrystals, in which L-glutamic acid (L-Glu) has been used to replace oleic acid in the synthetic process. Benefiting from the synergic effects of L-Glu and oleylamine (OAm), $CsPbBr_3$ nanocrystals (L-Glu/OAm-$CsPbBr_3$ NCs) with high water stability have been directly prepared under a mild condition at room temperature in water, facilitated by the process of crystal phase transformation from Cs_4PbBr_6 to $CsPbBr_3$. L-Glu/OAm-$CsPbBr_3$ NCs exhibit a high quantum yield of 85% and a narrow full width at half maximum of 16 nm, demonstrating their efficient luminescence in water. Typically, L-Glu on the surface have contributed greatly to an acidic environment and passivation of surface defects, improving the water stability and dispersibility of $CsPbBr_3$ nanocrystals. Moreover, L-Glu/OAm-$CsPbBr_3$ NCs exhibit great biocompatibility due to the presence of L-Glu, resulting in their good performance for HeLa cell imaging. Thus, we propose a facile and effective method to prepare $CsPbBr_3$ nanocrystals with excellent water stability by using L-Glu and OAm as cooperated ligands and expand their application in cell imaging.

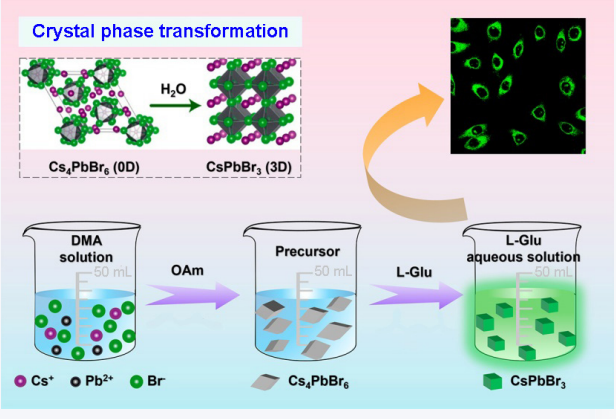

KEYWORDS: aqueous synthesis, cell imaging, lead halide perovskite nanocrystals, L-glutamic acid, phase transformation

1 Introduction

Lead halide perovskite nanocrystals (LHP NCs) have attracted significant interests due to their exceptional photoelectronic properties, including narrow half-peak width, high quantum yields, and tunable emission [1–6]. Thus, LHP NCs are proved to have great potentials for applications in the fields of light-emitting diodes [7, 8], liquid crystal displays [9], solar cells [10, 11], lasers [12, 13], photoelectric detection [14, 15] and bioimaging [16–19]. Especially for imaging of cells and tissues, there still remain the challenges including degraded image quality, light scattering, spontaneous fluorescent interference and reduced resolution due to complex morphological structures. The luminous advantage of LHP NCs shows their potential for application in biological imaging. However, there is a main obstacle, i.e., the poor stability and dispersibility in aqueous solution arising from their inherent ionicity and low energy of formation, which has largely restricted their practical applications [20–22]. The degradation of LHP NCs can be commonly observed when they are exposed to the environments with light, high-temperature, oxygen and moisture [23–27]. Since the stability of LHP NCs is an intractable problem that needs to be eagerly addressed, various methods have also been developed, such as surface passivation, ion doping and matrix encapsulation [28–31]. Nevertheless, these strategies often require complicated post-modification that results in degradation of nanocrystals and undesirable optical performance [32]. Moreover, the hot injection, ligand-assisted reprecipitation, solvothermal

Received: July 3, 2024; **Revised:** October 8, 2024
Accepted: October 11, 2024

✉Address correspondence to Yu Tang, tangyu@lzu.edu.cn; Nan Song, songn@lzu.edu.cn

method and ultrasonic method often suffer the problems of tedious procedures, harsh conditions (such as high temperatures, inert gases) or the toxic solvents (such as toluene) [3, 33–35], even they are the classical and well-known synthetic methods for LHP NCs. The hydrophobic ligands with long chains always close the surface of nanocrystals and cause the poor dispersion in polar solvents, which largely impede their production [36, 37].

Typically, the aqueous synthesis, as a green and gentle method, has been widely employed in preparation of chalcogenide semiconductor nanocrystals, which has significantly expanded their applications in biological environment. However, since the water molecules can decompose the LHP NCs and quench fluorescence, it is still kept in challenge to maintain the stability of their structures and fluorescent efficiency. As a result, the important role of water in the synthetic process has been continuously investigated [38, 39]. The introduction of trace water can control the environment of crystallization, further regulating their size, morphology, and optical properties [40]. And then, the water-stable $CH_3NH_3PbX_3$ nanocrystals could also be directly synthesized in the acidic medium [41], demonstrating that the pH value of aqueous solution could influence the charge of surface and equilibrium of dissolution. For instance, $CsPbX_3$ NCs could be synthesized and stabilized in aqueous solution via the *in-situ* preparation by using 4-bromobutyric acid [42] and 5-bromovaleric acid [43] as the substituted ligands instead of oleic acid. Further evidence has also indicated that water could induced the phase transition of LHP NCs from Cs_4PbX_6 to $CsPbX_3$, benefiting from their inherent soft lattices [44]. To synthesize inorganic lead halide perovskite $CsPbX_3$ (X = Cl, Br and I), the aqueous phase synthesis is still in infancy. Except direct synthetic methods in aqueous media, the post-synthetic conversion has also been widely reported to prepare the LHP NCs [45–47]. Some biomolecules, such as proteins, peptides, carbohydrates, nucleotides, etc, have been used as ligands for LHP NCs after substitution and proved to enhance their stability, luminescence, conductivity, and biocompatibility properties [48–52]. Compared with proteins and polypeptides with complex structures, different folding degree and diverse spiral mode, amino acids would exhibit significant advantages to promote the aqueous media syntheses of LHP NCs. Amino acids have simple and clear structures, which would be helpful to study the specific effects of structures and the synthetic mechanism. This post-synthesized transformation also inspired us to directly synthesize $CsPbBr_3$ nanocrystals in aqueous media, which is significant not only to develop the facile aqueous synthesis but also to realize their applications in biological fields.

Amino acids can be used to directly synthesize $CsPbBr_3$ nanocrystals instead of post-synthetic conversion. Herein, considering the synergistic effects of ligands and acid aqueous environment could potentially facilitate the stabilization of $CsPbBr_3$ nanocrystals, L-glutamic acids (L-Glu), as a biocompatible and acidic amino acid, could be selected as the ligands for the surface modification. L-Glu could not only provide the acidic aqueous media but also passivate the surface defects of nanocrystals. Besides, the water-triggered crystal phase transition from Cs_4PbBr_6 to $CsPbBr_3$ can be also realized. As consequence, by using L-Glu and oleylamine (OAm) as the cooperated ligands, the highly-stable and well-dispersed $CsPbBr_3$ nanocrystals with efficient luminescence could be easily obtained, which retained in aqueous solution and avoided the structural degradation for 88 h. Importantly, the double ligand-stabilized $CsPbBr_3$ nanocrystals, i.e., L-Glu/OAm-$CsPbBr_3$ NCs, could be applied for the cell imaging. This work provides a new idea for the exploration of facile methods to prepare highly stable $CsPbBr_3$ nanocrystals with excellent optical performance in aqueous media, especially those for biological applications.

2 Results and discussion

As depicted in Fig. 1(a), a facile and environment-friendly synthetic method was developed to effectively obtain water-stable $CsPbBr_3$ nanocrystals in aqueous media, which was facilitated by an

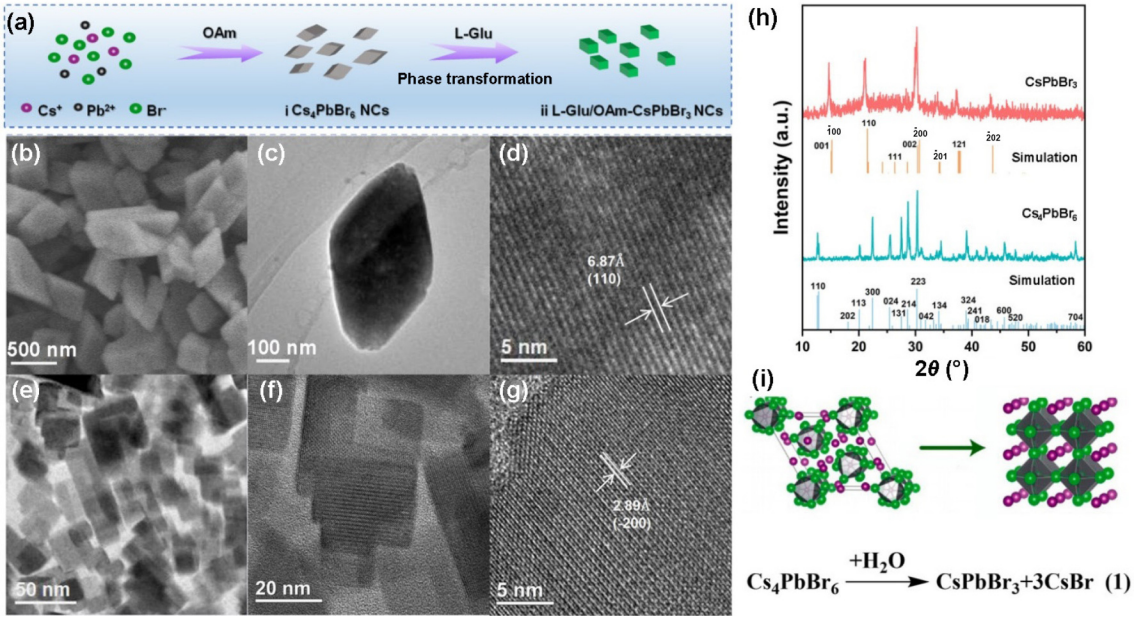

Figure 1 (a) Schematic illustration of the synthetic route and phase transformation process of L-Glu/OAm-$CsPbBr_3$ NCs. (b) SEM (scale bar: 500 nm), (c) TEM (scale bar: 100 nm) and (d) HRTEM (scale bar: 5 nm) images of the Cs_4PbBr_6 precursor. (e, f) TEM (scale bar: 50 nm in (e), 20 nm in (f)) and (g) HRTEM (scale bar: 5 nm) images of L-Glu/OAm-$CsPbBr_3$ NCs. (h) XRD spectra of Cs_4PbBr_6 precursor (blue line) and L-Glu/OAm-$CsPbBr_3$ NCs (red line) compared to their corresponding spectra of standard power diffraction patterns. (i) Schematic illustration of the crystal transformation from Cs_4PbBr_6 to $CsPbBr_3$ in water.

interesting water-induced post-synthetic transformation process of Cs_4PbBr_6 to $CsPbBr_3$. Firstly, Cs_4PbBr_6 precursor was synthesized by using a mild approach in the presence of OAm. The addition of an appropriate amount of OAm to N,N-dimethylacetamide (DMA) dissolved with equimolar CsBr and $PbBr_2$ could initiate the reaction, resulting in white precipitates. According to the previous literatures, excess OAm promotes the formation of Cs_4PbBr_6 phase, which is negligibly influenced by the ratio of Cs/Pb [45, 53]. Besides, the rhombohedral shaped particles of Cs_4PbBr_6 with an average diameter of 430 nm × 600 nm could be observed by both scanning electron microscope (SEM) and transmission electron microscopy (TEM) images (Figs. 1(b) and 1(c)). As depicted in Fig. 1(d) of the high-resolution transmission electron microscopy (HRTEM) image, the *d*-spacing of Cs_4PbBr_6 precursor was measured to be 6.87 Å, which was consistent with the (110) plane of rhombohedral Cs_4PbBr_6 precursor [54]. The formation of Cs_4PbBr_6 was also demonstrated by the ultraviolet–visible (UV–Vis) spectra in Fig. S1 in the Electronic Supplementary Material (ESM), where a sharp absorption peak at 315 nm could be aligned to its bulk films [55]. Furthermore, the SEM images and X-ray diffraction (XRD) patterns of Cs_4PbBr_6 precursors synthesized by OAm, dodecylamine and octylamine, respectively, demonstrated that the substitution with other amines with short hydrocarbon chains could also facilitate the formation of Cs_4PbBr_6 precursor (Figs. S2 and S3 in the ESM).

After fully characterization, the Cs_4PbBr_6 precursor was added to an aqueous solution of L-Glu dropwise with vigorous stirring and L-Glu/OAm-$CsPbBr_3$ NCs were successfully synthesized. The rapid reaction was realized through observing a distinct change from colorless to yellow-green, accompanied by strong green fluorescence upon irradiation under the ultraviolet lamp of 365 nm (Video S1 in the ESM). According to previous reports, this process is attributed to the high solubility of CsBr in water, which is stripped from the lead-rich Cs_4PbBr_6 precursor [56]. As shown in Figs. 1(e)–1(g), stacked square morphologies of L-Glu/OAm-$CsPbBr_3$ NCs could be observed with the size of 20–50 nm and *d*-spacing of 2.89 Å. In addition, the average diameter of L-Glu/OAm-$CsPbBr_3$ NCs was detected to be 130 nm by dynamic light scattering (DLS, Fig. S4 in the ESM), which was smaller than that was measured in TEM images. It was for the reason that DLS measures the hydration radius, whereas TEM measurement is in vacuum. Moreover, the crystal plane (110) of rhombohedral phase in Cs_4PbBr_6 precursor and crystal plane (200) in L-Glu/OAm-$CsPbBr_3$ NCs were both confirmed by XRD analysis (Fig. 1(h)), in accordance with their *d*-spacing of 6.87 and 2.89 Å in HRTEM images, respectively. Accordingly, the phase transformation from Cs_4PbBr_6 to $CsPbBr_3$ in aqueous solution was successfully testified and the process was also illustrated as an equation (Fig. 1(i)). As reported in the previous studies, $CsPbBr_3$ nanocrystals obtained through water-induced phase transformation often exhibit undesirable structural breakage and diminished luminescence upon further exposure to water [56, 57]. Therefore, only trace amount of water can be introduced into the synthetic process to establish a water–oil interface and facilitate the entering of nanocrystals to the non-polar solvent. With good fortune, the direct phase transformation from Cs_4PbBr_6 to $CsPbBr_3$ was successfully realized via this amino acid assisted synthetic strategy in aqueous media to avoid this drawback. Furthermore, the as-prepared L-Glu/OAm-$CsPbBr_3$ NCs exhibited extremely high water-stability and excellent luminescent properties in aqueous solution due to the synergic effect of ligands and acidic environment.

Subsequently, Fourier transform infrared (FTIR) and ^{1}H nuclear magnetic resonance (^{1}H NMR) were conducted to further investigate the role of ligands in improving the water stability. As shown in Fig. 2(a) of FTIR spectra, an emerged peak at 1400 cm^{-1} corresponding to the symmetric stretching vibration of COO^- could be observed in L-Glu/OAm-$CsPbBr_3$ NCs, indicating the presence of L-Glu on the surface of nanocrystals. In addition, the peak at 1625 cm^{-1} attributed to NH_3^+ was significantly enhanced, while the peak at 1570 cm^{-1} attributed to the bending vibration of NH_2 was attenuated [58]. This result could be ascribed to the protonation of NH_2 under acidic condition. Accordingly, OAm can immobilize to the surface of perovskite nanocrystals by protonating amino group to obtain NH_3^+ and then to form hydrogen bonding with Br^- on the surface [22, 59]. Furthermore, ^{1}H NMR spectrum shown in Fig. 2(b) also confirmed the binding of ligands on the surface of $CsPbBr_3$ nanocrystals. The three peaks at 3.45, 2.00 and 1.54 ppm were the hydrogens 1, 2 and 3 of L-Glu. Meanwhile, the presence of OAm is also confirmed by ^{1}H NMR. The peak at 5.35 ppm corresponded to the alkene proton 6 of oleylamine. As aforementioned, it could be concluded that the presence of surface L-Glu and OAm synergistically facilitated the protection of nanocrystals during crystal phase transition, ensuring their excellent dispersion and stability in aqueous media.

The luminescent properties of the L-Glu/OAm-$CsPbBr_3$ NCs were also testified. As depicted in Fig. 3(a), L-Glu/OAm-$CsPbBr_3$

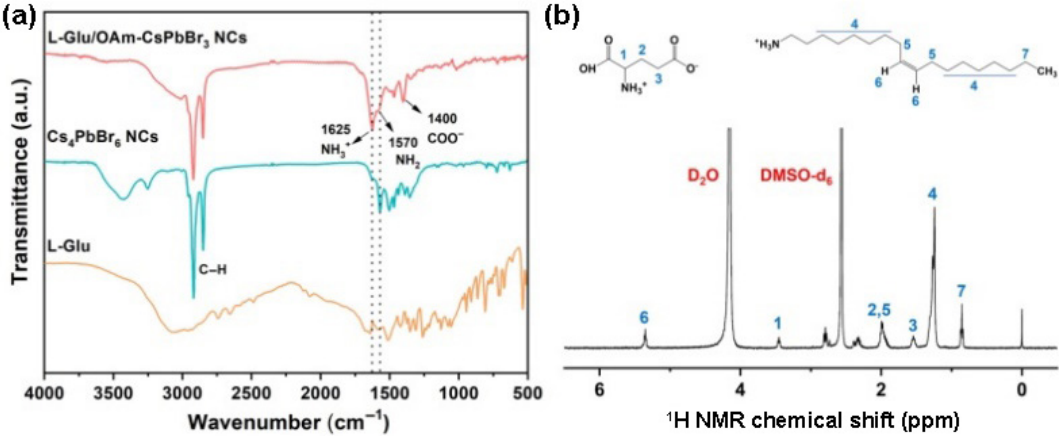

Figure 2 (a) Fourier transform infrared spectra of L-Glu/OAm-$CsPbBr_3$ NCs (red line), Cs_4PbBr_6 (blue line) and L-Glu ligand (yellow line). (b) ^{1}H NMR of L-Glu/OAm-$CsPbBr_3$ NCs (V(DMSO-d_6):V(D_2O) = 3:1, 298 K, 400 MHz).

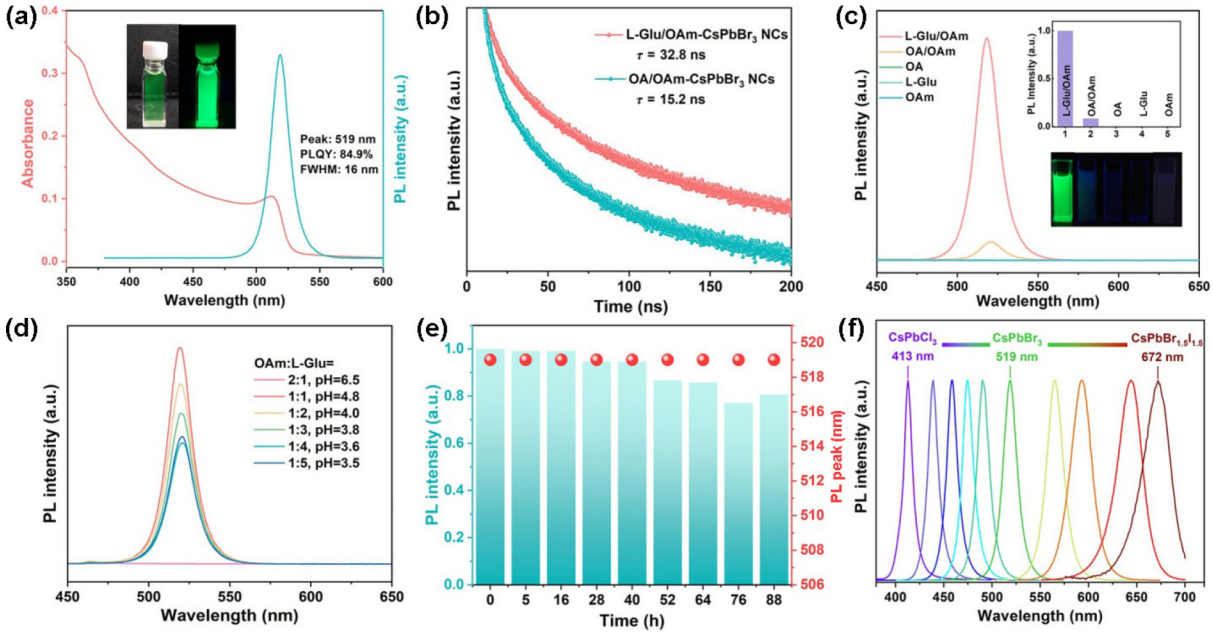

Figure 3 (a) UV–Vis absorption and photoluminescent spectrum of L-Glu/OAm-$CsPbBr_3$ NCs in aqueous solution. (b) Fluorescent lifetimes of OA/OAm-$CsPbBr_3$ nanocrystals synthesized through conventional methods and L-Glu/OAm-$CsPbBr_3$ NCs prepared via aqueous synthesis. (c) Fluorescent spectra of nanocrystals synthesized with different ligand combinations. (d) Fluorescent spectra of L-Glu/OAm-$CsPbBr_3$ NCs in solutions with various pH values and different ratios of OAm and L-Glu. (e) The fluorescent intensity of L-Glu/OAm-$CsPbBr_3$ NCs in aqueous media for different time. (f) Fluorescent spectra of $CsPbX_3$ nanocrystals with different halogens.

NCs exhibited an absorption at 511 nm and a narrow fluorescent emission at the peak of 519 nm. The solution of L-Glu/OAm-$CsPbBr_3$ NCs exhibited a green transparent appearance, indicating the excellent dispersity in water. Besides, the zeta potentials of L-Glu/OAm-$CsPbBr_3$ NCs also confirmed their good dispersity (Fig. S5 in the ESM). Moreover, L-Glu/OAm-$CsPbBr_3$ NCs also possessed a high color purity of 16 nm and remarkably high quantum yield of 85%, indicating the excellent photoluminescence in aqueous media. The time-resolved photoluminescence decay curve of L-Glu/OAm-$CsPbBr_3$ NCs revealed its average lifetime of 32.8 ns fitted with a bi-exponential function (Fig. 3(b)), which was longer than that of traditional OA/OAm-$CsPbBr_3$ NCs (15.2 ns). According to the previous literature, the longer fluorescence lifetime indicates the reduced surface defects to capture charge carriers [38]. This indicated that L-Glu/OAm-$CsPbBr_3$ NCs exhibited reduced surface defects, resulting from the passivation effect of L-Glu. The prolonged fluorescent lifetime of L-Glu/OAm-$CsPbBr_3$ NCs suggested that the defect passivation could eliminate the trap-assisted non-radiative recombination [14]. In order to elucidate the indispensable roles of OAm and L-Glu in stabilizing $CsPbBr_3$ nanocrystals, various ligands including OA, OAm, and L-Glu were used as ligands in the manner of different combinations. The fluorescent spectra and photographs in Fig. 3(c) demonstrated that L-Glu/OAm-$CsPbBr_3$ NCs could disperse stably in aqueous solution and exhibit strong green emission because of the synergic effect of OAm and L-Glu. As comparison, the white precipitates with negligible fluorescent emission were obtained with other ligands such as OA/OAm, individual OA, L-Glu and OAm. Additionally, the stable solution of L-Glu/OAm-$CsPbBr_3$ NCs could be always obtained even upon continuously increasing the L-Glu with the molar ratio of OAm/L-Glu from 2:1 to 1:5. Thus, OAm and L-Glu were testified to have synergic effect in stabilization of $CsPbBr_3$ nanocrystals at aqueous solution.

Typically, L-Glu exhibited the capacity of buffering due to the zwitterionic properties, which allows its aqueous solution to maintain acidic (pH = 3.5–5.0) upon adding the Cs_4PbBr_6 precursor containing OAm [60]. Thus, as shown in Fig. 3(d) and Fig. S6 in the ESM, the pH values of the solution were measured to be changed from 6.5 to 3.5, upon adjusting the molar ratio of OAm/L-Glu from 2:1 to 1:5. As consequence, L-Glu/OAm-$CsPbBr_3$ NCs could not stably exist and white precipitate was obtained at the neutral condition (pH = 6.5), when L-Glu was at relatively low concentration (OAm/L-Glu = 2:1).

Furthermore, the controllable crystal phase transformation was also found to have a certain correlation with pH values of solution. Remarkably, the fluorescent emission intensity of L-Glu/OAm-$CsPbBr_3$ NCs maintained strong as above 80% of its initial intensity even after 88 h, indicating its excellent stability (Fig. 3(e)). The slight decrease of fluorescent intensity indicated a gradual degradation of L-Glu/OAm-$CsPbBr_3$ NCs, causing by their partial transformation into non-luminous $CsPb_2Br_5$. The previous studies have already highlighted the superior stability of $CsPb_2Br_5$ in aqueous media [61]. Subsequently, a wide ranging of photoluminescent emission covering almost visible area (at the wavelengths from 413 to 672 nm) could be tuned upon varying the halide composition of the Cs_4PbX_6 precursor (Fig. 3(f)). The crystal transformation from Cs_4PbX_6 to $CsPbX_3$ (X = Cl, Br, Cl/Br, Br/I) was successfully achieved through this acid-assisted synthetic strategy (Figs. S7 and S8 in the ESM). The narrow, single-peak photoluminescent emissions with a full wavenlengths at half maximum of 10–40 nm were observed, suggesting the nanocrystals dispersed in aqueous solutions possessed the uniform distribution. Nevertheless, the pure $CsPbI_3$ nanocrystals could not be synthesized via this method, because of their worse structural stability. As demonstrated above, this acid-assisted aqueous synthesis was a general method to prepare $CsPbX_3$ nanocrystals with different halide composition in aqueous media, solving the problem of that lead halide perovskite nanocrystals were susceptible to degradation when exposed to water.

A recent research has revealed that the alkylammonium ligands are incorporated into certain sites of Cs ions, while the carboxyl groups tend to be adsorbed onto the surface by coordinated with the Cs atoms [62]. Accordingly, the mechanism of the cooperated effect of L-Glu and OAm to improve the stability of $CsPbBr_3$ NCs was also studied by the density functional theory (DFT) calculations (Figs. 4(a)–4(c)). DFT results demonstrated that there was a binding energy of 1.67 eV on the surface of L-Glu/OAm-$CsPbBr_3$ NCs, which was much higher than that of both OA/OAm-$CsPbBr_3$ NCs ($E_{binding}$ = 0.87 eV) and OAm-$CsPbBr_3$ NCs ($E_{binding}$ = 0.74 eV). Therefore, this result of theoretical calculation also confirmed that L-Glu and OAm could cooperatively enhance the stability of $CsPbBr_3$ nanocrystals in aqueous solution.

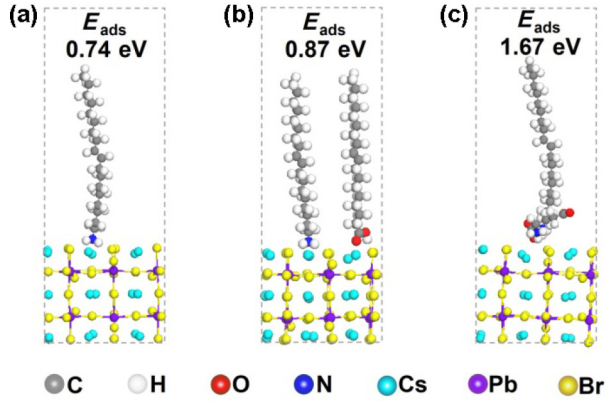

Figure 4 The binding model and DFT calculation results of (a) OAm, (b) OA/OAm and (c) L-Glu/OAm modified on surface of $CsPbBr_3$ nanocrystals.

Further investigation was also conducted to elucidate the impact of different ligands on the synthesis and stability of $CsPbBr_3$ nanocrystals. Amino acids are organic compounds containing amino groups and acidic carboxyl groups, which can be divided into four categories including non-polar, polar neutral, acidic and basic amino acids. Thus, seven different hydrosoluble amino acids were introduced to evaluate the role of amino acids in the synthetic process, such as L-Glutamic acid (L-Glu), L-Aspartate (L-Asp), L-Cysteine (L-Cys), L-Serine (L-Ser), L-Threonine (L-Thr), L-Histidine (L-His), and L-Arginine (L-Arg). Only acidic amino acids (L-Glu and L-Asp) could realize the successful aqueous synthesis of $CsPbBr_3$ nanocrystals with stable dispersion and efficient fluorescence (Figs. S9 and S10, and Table S1 in the ESM). Acidic amino acids have carboxylic groups that are completely ionized with the isoelectric point of 3, which makes their solution to be acidic [60]. However, other types of amino acids cannot facilitate the synthesis of $CsPbBr_3$ nanocrystals by using this strategy due to their higher isoelectric points even with similar functional groups to acidic amino acids, because they resulted in neutral or alkaline environment. Consequently, it suggested that the acidic environment played a crucial role in aqueous synthesis and phase transformation. In addition, to further verify the necessity of zwitterionic structures in L-Glu for the successful synthesis, acidic Boc-L-Glu with α-amino-protecting groups was also used to prepare $CsPbBr_3$ NCs. Boc-L-Glu/OAm-$CsPbBr_3$ NCs exhibited rapidly quenching of fluorescence within 5 min (Fig. S11 in the ESM). It demonstrated that zwitterionic structure of L-Glu, i.e., the ammonium cation and carboxylate anion to either dissociate hydrogen ions or accept protons, was also important to synthesize $CsPbBr_3$ NCs in this strategy. We conducted additional experiments to assess the change of photoluminescence (PL) intensity of L-Asp/OAm-$CsPbBr_3$ NCs over a prolonged period. The fluorescent intensity decayed to about 50% of its initial level after 60 h (Fig. S12 in the ESM), which indicated the less stability of L-Asp/OAm-$CsPbBr_3$ NCs compared with L-Glu/OAm-$CsPbBr_3$ NCs in water media. Furthermore, n-octylamine and dodecylamine were selected to replace OAm, demonstrating that the amine groups could facilitate the formation of Cs_4PbBr_6 precursor. However, the fluorescence of $CsPbBr_3$ nanocrystals stabilizing by n-octylamine was transient, lasting only a few seconds before rapidly extinguishing. It is evident that amine ligands with longer chain had poor solubility in water. Thus, OAm acted as the hydrophobic shell to effectively protect the nanocrystalline from degradation. Besides, the protons in water facilitated the protonation of $-NH_2$ to be $-NH_3^+$, which strongly bond to Br^- on the surface of nanocrystals.

Other types of acids, such as inorganic acids (HBr, HNO_3, H_2SO_4 and H_3PO_4) and organic acids (CHOOH and CH_3COOH) were selected to further investigate the important role of acidic environment during the process of synthesis. The $CsPbBr_3$ nanocrystals with vivid green emission could be obtained in the acidic solution of HBr, HNO_3, and CHOOH and CH_3COOH with appropriate pH (Figs. S13 and S14 in the ESM), while they were failed to be synthesized in the aqueous solution of H_2SO_4 or H_3PO_4. It could be ascribed to the high solubility product constant (K_{sp}) values of $PbSO_4$ and $Pb_2(PO_4)_3$. And then, L-Glu/OAm-$CsPbBr_3$ NCs were dispersed in the aqueous solutions of HBr with pH values of 1.0, 2.0, 3.0, 4.0, and 5.0, respectively. L-Glu/OAm-$CsPbBr_3$ NCs exhibited the best stability when the pH value was 2.0 (Figs. S15 and S16 in the ESM). In order to demonstrate the significance of acidic environment in avoiding the degradation of $CsPbBr_3$ nanocrystals in water, OA/OAm-$CsPbBr_3$ quantum dots (QDs) were also synthesized by the hot-injection method. The $CsPbBr_3$ QDs were dispersed in the toluene solution and then vigorously mixed with varying acidic solutions (Fig. S17 in the ESM). Upon interaction with water, OA/OAm-$CsPbBr_3$ QDs were almost degraded and completely transformed into a white emulsion with weak green fluorescence. Nevertheless, OA/OAm-$CsPbBr_3$ QDs with bright green fluorescence could be stabilized when they were in acidic solutions. Rapid fluorescent quenching was also observed when triethanolamine was added to adjust the aqueous solution of L-Glu/OAm-$CsPbBr_3$ NCs into alkalinity (Fig. S18 in the ESM). All of above results demonstrated that acidic environment played a dominant role in the synthesis and stabilization of L-Glu/OAm-$CsPbBr_3$ NCs.

As L-Glu/OAm-$CsPbBr_3$ NCs were synthesized in aqueous media assisted by acidic amino acids and exhibited excellent luminescent stability, it was envisaged to have great potentials as bio-probes. Therefore, the cytotoxicity of L-Glu/OAm-$CsPbBr_3$ NCs were assessed on HeLa and HUVEC cells by using cell counting kit-8 assay (CCK-8). The cellular viabilities were estimated to be about 80% upon incubating L-Glu/OAm-$CsPbBr_3$ NCs with cells for 8 h (Fig. 5(a)), demonstrating the good biocompatibility of L-Glu/OAm-$CsPbBr_3$ NCs. Significant cellular toxicity was observed in normal cells when the concentration exceeds 40 μg/mL. Moreover, the green emission of L-Glu/OAm-$CsPbBr_3$ NCs could be observed in HeLa cells upon being excited by the light at wavelength of 400 nm. The fluorescence was enhanced upon incubating them for 6 h and maintained for 24 h even there was attenuation of intensity, indicating that L-Glu/OAm-$CsPbBr_3$ NCs exhibited a good performance in tracking of cells (Fig. 5(b) and Fig. S19 in the ESM).

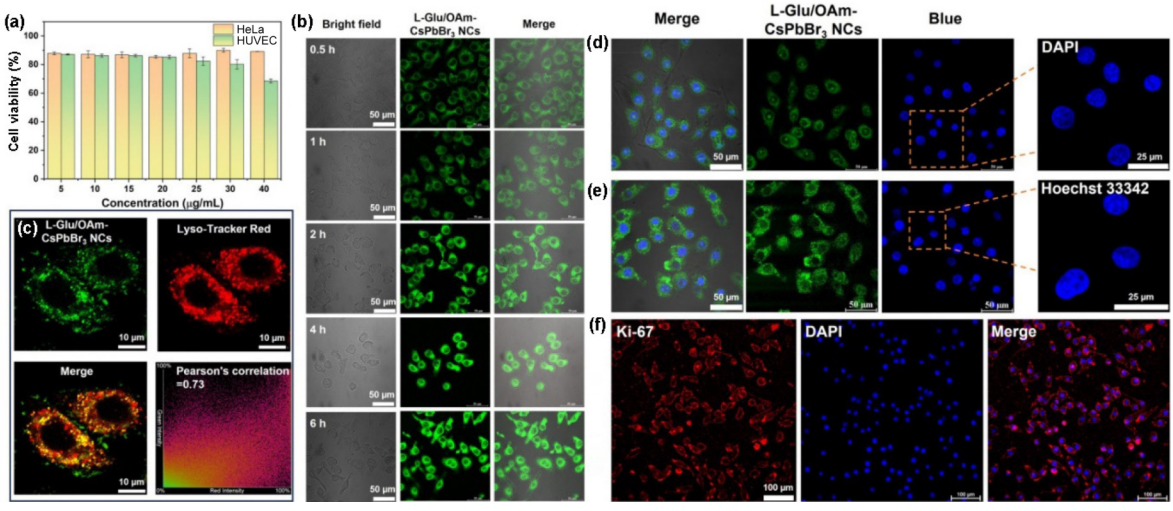

Figure 5 (a) Viability of HeLa cells treated with different concentrations of L-Glu/OAm-$CsPbBr_3$ NCs. (b) CLSM images of cells incubated with L-Glu/OAm-$CsPbBr_3$ NCs for 0.5–6 h (λ_{ex} = 400 nm). (c) CLSM images with high-resolution (the cells incubated with L-Glu/OAm-$CsPbBr_3$ NCs, Lyso-Tracker Red and their merged image) and the Pearson's correlation of L-Glu/OAm-$CsPbBr_3$ NCs (green) with lysosomes (red) after incubation for 1 h. CLSM images of HeLa cells incubated with L-Glu/OAm-$CsPbBr_3$ NCs (40 μg/mL) and stained with (d) DAPI, (e) Hoechst 33342 and (f) Ki67 (immunofluorescence, red, mouse monoclonal antibody).

According to the cell staining experiments performed on a confocal laser scanning microscope (CLSM), L-Glu/OAm-$CsPbBr_3$ NCs was internalized into cells within 1 h and then entrapped into lysosomes with a Pearson's correlation coefficient of 0.73 (Fig. 5(c)). This targeting could be ascribed to the acidic environment in lysosome, which provided their favorable acidic condition for the stability of L-Glu/OAm-$CsPbBr_3$ NCs. To further assess the impact of nanocrystals on DNA integrity, HeLa cells were stained by using DAPI and Hoechst 33342 after incubating with L-Glu/OAm-$CsPbBr_3$ NCs for 8 h. DAPI and Hoechst 33342 are markers to specifically bind with nuclear DNA. As depicted in Figs. 5(d) and 5(e), robust blue fluorescence within nuclei was observed in CLSM images, indicating the intact morphologies of nucleis. Thus, the nanocrystals did not destroy the DNA integrity of cells. Furthermore, Ki67 cell proliferation assay kit was used to stain HeLa cells. The expression of Ki67 can assess the proliferative state of cells. As shown in Fig. 5(f) and Fig. S20 in the ESM, the HeLa cells were incubated with nanocrystals for 8, 24, 48 and 72 h, respectively. The strong red fluorescence indicated the high expression Ki67 associated with cell proliferation. It was found that the proliferation of HeLa cells was still good even after 72 h incubation. The above results demonstrated that the enrichment of L-Glu/OAm-$CsPbBr_3$ NCs in cells had no side effect on both DNA integrity and cell proliferation. All of the good biocompatibility, cell tracking and lysosome targeting of L-Glu/OAm-$CsPbBr_3$ NCs indicated their broad prospect in biological applications. In order to evaluate the potential applications *in vivo*, we investigated the fluorescence stability of L-Glu/OAm-$CsPbBr_3$ NCs in simulated gastric juices (Fig. S21 in the ESM). Since the main component of gastric juice is hydrochloric acid, the anion exchange of L-Glu/OAm-$CsPbBr_3$ NCs tended to be occurred. Thus, L-Glu/OAm-$CsPbBr_3$ NCs exhibited a blue shift. The luminescence of L-Glu/OAm-$CsPbBr_3$ NCs is gradually blue shift within 10 min, accompanied by a decrease in luminescence intensity. Considering the same chloride ion, L-Glu/OAm-$CsPbCl_3$ NCs have also been used to investigated the behaviors in gastric juices. Owing to the acidic environment of the gastric fluid (pH = 1.5), the fluorescence of $CsPbCl_3$ NCs was ever-present even after 60 h. It also shows that this material has the potential of imaging in the stomach.

3 Conclusions

In summary, the poor water stability of LHP NCs has largely limited their applications in biological fields. In order to tackle this challenge, L-Glu/OAm-$CsPbBr_3$ NCs were successfully prepared in aqueous solution via a facile method with an interesting process of post-crystal transformation. The amino acid of L-Glu was used as the ligand in cooperation with OAm to provide the acidic environment and passivate the surface defects of $CsPbBr_3$ nanocrystals. L-Glu/OAm-$CsPbBr_3$ NCs exhibited excellent luminescent properties, such as narrow full width at half maximum (FWHM), high quantum yield and adjustable fluorescence. Moreover, they also exhibited improved water stability. Besides, the effect of acidic amino acids as the ligands to stabilize $CsPbBr_3$ nanocrystals has been fully studied, confirming the crucial role of acidic environment in the synthetic process. Benefiting from the good biocompatibility of amino acids, L-Glu/OAm-$CsPbBr_3$ NCs had good performance in cell imaging with a tracking time for more than 24 h. We anticipate that more environment-friendly and facile methods to prepare of LHP NCs could be proposed and developed by inspiration of this study. With this method, various ligands could be developed. The LHP NCs with high stability and efficient luminescence could be synthesized, which would be applied for long-term tracking or precise monitoring in biological systems.

Electronic Supplementary Material: Supplementary materials (materials and methods; detailed characterizations of Cs_4PbBr_6 precursor, including the UV–Vis spectra, XRD patterns, SEM images, etc; fluorescent spectra of $CsPbBr_3$ nanocrystals with different ligands and pH values; the fluorescence of $CsPbBr_3$ nanocrystals in different acids; CLSM images of cells incubated with L-Glu/OAm-$CsPbBr_3$ NCs for 12 and 24 h, respectively) is available in the online version of this article at https://doi.org/10.26599/NR.2025.94907067.

Data availability

All data needed to support the conclusions in the paper are presented in the manuscript and the Electronic Supplementary

Material. Additional data related to this paper may be requested from the corresponding author upon request.

Acknowledgements

We acknowledge the financial support from the National Natural Science Foundation of China (Nos. 22221001, and 22131007), the Science and Technology Major Plan of Gansu Province (No. 23ZDGA012), and the 111 project (No. B20027).

Declaration of competing interest

All the contributing authors report no conflict of interests in this work.

Author contribution statement

X. L.: Experimental design, data curation and writing manuscript. Y. N. G.: Cellular experimental design and conduction. G. Y. T.: Density functional theory (DFT) calculations. Q. Y. L.: Validation. N. S.: Experimental design and writing manuscript. Y. T.: Project administration, funding acquisition and writing manuscript. All the authors have approved the final manuscript.

Informed consent

Not applicable.

Ethics statement

Not applicable.

Use of AI statement

None.

References

[1] Kovalenko, M. V.; Protesescu, L.; Bodnarchuk, M. I. Properties and potential optoelectronic applications of lead halide perovskite nanocrystals. *Science* **2017**, *358*, 745–750.

[2] Shamsi, J.; Urban, A. S.; Imran, M.; De Trizio, L.; Manna, L. Metal halide perovskite nanocrystals: Synthesis, post-synthesis modifications, and their optical properties. *Chem. Rev.* **2019**, *119*, 3296–3348.

[3] Protesescu, L.; Yakunin, S.; Bodnarchuk, M. I.; Krieg, F.; Caputo, R.; Hendon, C. H.; Yang, R. X.; Walsh, A.; Kovalenko, M. V. Nanocrystals of cesium lead halide perovskites ($CsPbX_3$, X = Cl, Br, and I): Novel optoelectronic materials showing bright emission with wide color gamut. *Nano Lett.* **2015**, *15*, 3692–3696.

[4] Manser, J. S.; Christians, J. A.; Kamat, P. V. Intriguing optoelectronic properties of metal halide perovskites. *Chem. Rev.* **2016**, *116*, 12956–13008.

[5] Dutta, A.; Behera, R. K.; Pal, P.; Baitalik, S.; Pradhan, N. Near-unity photoluminescence quantum efficiency for all $CsPbX_3$ (X=Cl, Br, and I) perovskite nanocrystals: A generic synthesis approach. *Angew. Chem., Int. Ed.* **2019**, *58*, 5552–5556.

[6] Yoon, Y. J.; Lee, K. T.; Lee, T. K.; Kim, S. H.; Shin, Y. S.; Walker, B.; Park, S. Y.; Heo, J.; Lee, J.; Kwak, S. K. et al. Reversible, full-color luminescence by post-treatment of perovskite nanocrystals. *Joule* **2018**, *2*, 2105–2116.

[7] Zhang, L. Q.; Yang, X. L.; Jiang, Q.; Wang, P. Y.; Yin, Z. G.; Zhang, X. W.; Tan, H. R.; Yang, Y.; Wei, M. Y.; Sutherland, B. R. et al. Ultra-bright and highly efficient inorganic based perovskite light-emitting diodes. *Nat. Commun.* **2017**, *8*, 15640.

[8] Cao, Y. B.; Zhang, D. Q.; Zhang, Q. P.; Qiu, X.; Zhou, Y.; Poddar, S.; Fu, Y.; Zhu, Y. D.; Liao, J. F.; Shu, L. et al. High-efficiency, flexible and large-area red/green/blue all-inorganic metal halide perovskite quantum wires-based light-emitting diodes. *Nat. Commun.* **2023**, *14*, 4611.

[9] Lin, J. D.; Lu, Y. X.; Li, X. Y.; Huang, F.; Yang, C. B.; Liu, M. L.; Jiang, N. Z.; Chen, D. Q. Perovskite quantum dots glasses based backlit displays. *ACS Energy Lett.* **2021**, *6*, 519–528.

[10] Zhao, X. M.; Liu, T. R.; Burlingame, Q. C.; Liu, T. J.; Holley, R.; Cheng, G. M.; Yao, N.; Gao, F.; Loo, Y. L. Accelerated aging of all-inorganic, interface-stabilized perovskite solar cells. *Science* **2022**, *377*, 307–310.

[11] Huang, J.; Wang, H.; Jia, C. L.; Tang, Y. Z.; Yang, H. S.; Chen, C. Y.; Gou, K. Y.; Zhou, Y. F.; Zhang, D.; Liu, S. Z. Advances in crystallization regulation and defect suppression strategies for all-inorganic $CsPbX_3$ perovskite solar sells. *Prog. Mater Sci.* **2024**, *141*, 101223.

[12] Liu, N.; Luo, H. Y.; Wei, X. Y.; Zeng, X.; Yang, J.; Huang, Y. X.; Yu, P.; Wang, Y. P.; Zhang, D. K.; Pi, M. Y. et al. Linearly manipulating color emission via anion exchange technology for high performance amplified spontaneous emission of perovskites. *Adv. Mater.* **2024**, *36*, 2308672.

[13] Zhang, Q.; Shang, Q. Y.; Su, R.; Do, T. T. H.; Xiong, Q. H. Halide perovskite semiconductor lasers: Materials, cavity design, and low threshold. *Nano Lett.* **2021**, *21*, 1903–1914.

[14] Bao, C. X.; Yang, J.; Bai, S.; Xu, W. D.; Yan, Z. B.; Xu, Q. Y.; Liu, J. M.; Zhang, W. J.; Gao, F. High performance and stable all-inorganic metal halide perovskite-based photodetectors for optical communication applications. *Adv. Mater.* **2018**, *30*, 1803422.

[15] Zhu, H. Y.; Chen, H. F.; Fei, J. J.; Deng, Y. T.; Yang, T.; Chen, P. H.; Liang, Y.; Cai, Y. Q.; Zhu, L.; Huang, Z. F. Solution-processed $CsPbBr_3$ perovskite films via CsBr intercalated $PbBr_2$ intermediate for high-performance photodetectors towards. *Nano Energy* **2024**, *125*, 109513.

[16] Cheng, L. J.; Chi, J. M.; Su, M.; Song, Y. L. Interface engineering of perovskite nanocrystals: Challenges and opportunities for biological imaging and detection. *J. Mater. Chem. C* **2023**, *11*, 7970–7981.

[17] Wang, S.; Wei, Z. Y.; Xu, Q.; Yu, L.; Xiao, Y. X. Trinity strategy: Enabling perovskite as hydrophilic and efficient fluorescent nanozyme for constructing biomarker reporting platform. *ACS Nano* **2024**, *18*, 1084–1097.

[18] Avugadda, S. K.; Castelli, A.; Dhanabalan, B.; Fernandez, T.; Silvestri, N.; Collantes, C.; Baranov, D.; Imran, M.; Manna, L.; Pellegrino, T. et al. Highly emitting perovskite nanocrystals with 2-year stability in water through an automated polymer encapsulation for bioimaging. *ACS Nano* **2022**, *16*, 13657–13666.

[19] Dong, Y. H.; Tang, X. Q.; Zhang, Z. W.; Song, J. Z.; Niu, T. C.; Shan, D.; Zeng, H. B. Perovskite nanocrystal fluorescence-linked immunosorbent assay methodology for sensitive point-of-care biological test. *Matter* **2020**, *3*, 273–286.

[20] Huang, H.; Bodnarchuk, M. I.; Kershaw, S. V.; Kovalenko, M. V.; Rogach, A. L. Lead halide perovskite nanocrystals in the research spotlight: Stability and defect tolerance. *ACS Energy Lett.* **2017**, *2*, 2071–2083.

[21] Yang, D. D.; Li, X. M.; Zeng, H. B. Surface chemistry of all inorganic halide perovskite nanocrystals: Passivation mechanism and stability. *Adv. Mater. Interfaces* **2018**, *5*, 1701662.

[22] De Roo, J.; Ibáñez, M.; Geiregat, P.; Nedelcu, G.; Walravens, W.; Maes, J.; Martins, J. C.; Van Driessche, I.; Kovalenko, M. V.; Hens, Z. Highly dynamic ligand binding and light absorption coefficient of

cesium lead bromide perovskite nanocrystals. *ACS Nano* **2016**, *10*, 2071–2081.

[23] Brennan, M. C.; Veghte, D. P.; Ford, B. R.; McCleese, C. L.; Loftus, L. M.; McComb, D. W.; Song, Z. N.; Heben, M. J.; Grusenmeyer, T. A. Photolysis of mixed halide perovskite nanocrystals. *ACS Energy Lett.* **2023**, *8*, 2150–2158.

[24] Li, Q. Y.; Shen, D. Y.; Luo, C. Z.; Zheng, Z. S.; Xia, W. L.; Ma, W. C.; Li, J.; Yang, Y. X.; Chen, S.; Chen, Y. Ultra-thermostability of spatially confined and fully protected perovskite nanocrystals by *in situ* crystallization. *Small* **2022**, *18*, 2107452.

[25] Straus, D. B.; Guo, S.; Abeykoon, A. M. M.; Cava, R. J. Understanding the Instability of the halide perovskite $CsPbI_3$ through temperature-dependent structural analysis. *Adv. Mater.* **2020**, *32*, 2001069.

[26] Wang, Z. Y.; Wei, Y. C.; Chen, Y. M.; Zhang, H. Y.; Wang, D.; Ke, J. X.; Liu, Y. S.; Hong, M. C. "Whole-Body" fluorination for highly efficient and ultra-stable all-inorganic halide perovskite quantum dots. *Angew. Chem. , Int. Ed.* **2024**, *63*, e202315841.

[27] Wang, J.; Long, R. Nuclear quantum effects accelerate charge recombination but boost the stability of inorganic perovskites in mild humidity. *Nano Lett.* **2024**, *24*, 3476–3483.

[28] Krieg, F.; Ong, Q. K.; Burian, M.; Rainò, G.; Naumenko, D.; Amenitsch, H.; Süess, A.; Grotevent, M. J.; Krumeich, F.; Bodnarchuk, M. I. et al. Stable ultraconcentrated and ultradilute colloids of $CsPbX_3$ (X = Cl, Br) nanocrystals using natural lecithin as a capping ligand. *J. Am. Chem. Soc.* **2019**, *141*, 19839–19849.

[29] Li, Y.; Wang, X. Y.; Xue, W. N.; Wang, W.; Zhu, W.; Zhao, L. J. Highly luminescent and stable $CsPbBr_3$ perovskite quantum dots modified by phosphine ligands. *Nano Res.* **2019**, *12*, 785–789.

[30] Li, S.; Shi, Z. F.; Zhang, F.; Wang, L. T.; Ma, Z. Z.; Yang, D. W.; Yao, Z. Q.; Wu, D.; Xu, T. T.; Tian, Y. T. et al. Sodium doping-enhanced emission efficiency and stability of $CsPbBr_3$ nanocrystals for white light-emitting devices. *Chem. Mater.* **2019**, *31*, 3917–3928.

[31] Lv, W. Z.; Li, L.; Xu, M. C.; Hong, J. X.; Tang, X. X.; Xu, L. G.; Wu, Y. H.; Zhu, R.; Chen, R. F.; Huang, W. Improving the stability of metal halide perovskite quantum dots by encapsulation. *Adv. Mater.* **2019**, *31*, 1900682.

[32] Li, Z. J.; Hofman, E.; Li, J.; Davis, A. H.; Tung, C. H.; Wu, L. Z.; Zheng, W. W. Photoelectrochemically active and environmentally stable $CsPbBr_3/TiO_2$ core/shell nanocrystals. *Adv. Funct. Mater.* **2018**, *28*, 1704288.

[33] Li, X. M.; Wu, Y.; Zhang, S. L.; Cai, B.; Gu, Y.; Song, J. Z.; Zeng, H. B. $CsPbX_3$ quantum dots for lighting and displays: Room-temperature synthesis, photoluminescence superiorities, underlying origins and white light-emitting diodes. *Adv. Funct. Mater.* **2016**, *26*, 2435–2445.

[34] Chen, M.; Zou, Y. T.; Wu, L. Z.; Pan, Q.; Yang, D.; Hu, H. C.; Tan, Y. S.; Zhong, Q. X.; Xu, Y.; Liu, H. Y. et al. Solvothermal synthesis of high-quality all-inorganic cesium lead halide perovskite nanocrystals: From nanocube to ultrathin nanowire. *Adv. Funct. Mater.* **2017**, *27*, 1701121.

[35] Tong, Y.; Bladt, E.; Aygüler, M. F.; Manzi, A.; Milowska, K. Z.; Hintermayr, V. A.; Docampo, P.; Bals, S.; Urban, A. S.; Polavarapu, L. et al. Highly luminescent cesium lead halide perovskite nanocrystals with tunable composition and thickness by ultrasonication. *Angew. Chem., Int. Ed.* **2016**, *55*, 13887–13892.

[36] Hills-Kimball, K.; Yang, H. J.; Cai, T.; Wang, J. Y.; Chen, O. Recent advances in ligand design and engineering in lead halide perovskite nanocrystals. *Adv. Sci.* **2021**, *8*, 2100214.

[37] Pan, A. Z.; He, B.; Fan, X. Y.; Liu, Z. K.; Urban, J. J.; Alivisatos, A. P.; He, L.; Liu, Y. Insight into the ligand-mediated synthesis of colloidal cspbbr3 perovskite nanocrystals: The role of organic acid, base, and cesium precursors. *ACS Nano* **2016**, *10*, 7943–7954.

[38] Zhang, M. Q.; Bi, C. H.; Xia, Y. X.; Sun, X. J.; Wang, X. Y.; Liu, A. Q.; Tian, S. Y.; Liu, X. F.; de Leeuw, N. H.; Tian, J. J. Water-driven synthesis of deep-blue perovskite colloidal quantum wells for electroluminescent devices. *Angew. Chem., Int. Ed.* **2023**, *62*, e202300149.

[39] Jin, X. D.; Wang, C. Q.; Miao, Y. Q.; Liu, P. Z.; Ji, J. L.; Chang, M. J.; Xu, B. S.; Zhao, M.; Tian, J. J.; Guo, J. J. In situ surface reconstruction in pure water by ice-confined freeze-thaw strategy for high-performance core–shell structural perovskite nanocrystals. *Adv. Funct. Mater.* **2024**, *34*, 2401435.

[40] Zhang, X. Y.; Bai, X.; Wu, H.; Zhang, X. T.; Sun, C.; Zhang, Y.; Zhang, W.; Zheng, W. T.; Yu, W. W.; Rogach, A. L. Water-assisted size and shape control of $CsPbBr_3$ perovskite nanocrystals. *Angew. Chem., Int. Ed.* **2018**, *57*, 3337–3342.

[41] Geng, C.; Xu, S.; Zhong, H. Z.; Rogach, A. L.; Bi, W. G. Aqueous synthesis of methylammonium lead halide perovskite nanocrystals. *Angew. Chem., Int. Ed.* **2018**, *57*, 9650–9654.

[42] Zhu, H.; Pan, Y. X.; Peng, C. D.; Lian, H. Z.; Lin, J. 4-Bromo-butyric acid-assisted *in situ* passivation strategy for superstable all-inorganic halide perovskite $CsPbX_3$ quantum dots in polar media. *Angew. Chem. , Int. Ed.* **2022**, *61*, e202116702.

[43] Song, S.; Lv, Y. C.; Cao, B. Q.; Wang, W. Z. Surface modification strategy synthesized $CsPbX_3$ perovskite quantum dots with excellent stability and optical properties in water. *Adv. Funct. Mater.* **2023**, *33*, 2300493.

[44] Yin, J. Y.; Zhang, J.; Wu, Z. Z.; Wu, F.; Li, X.; Dai, J. N.; Chen, C. Q. Origin of water-stable $CsPbX_3$ quantum dots assisted by zwitterionic ligands and sequential strategies for enhanced luminescence based on crystal evolution. *Small* **2024**, *20*, 2307042.

[45] Liu, Z. K.; Bekenstein, Y.; Ye, X. C.; Nguyen, S. C.; Swabeck, J.; Zhang, D. D.; Lee, S. T.; Yang, P. D.; Ma, W. L.; Alivisatos, A. P. Ligand mediated transformation of cesium lead bromide perovskite nanocrystals to lead depleted Cs_4PbBr_6 nanocrystals. *J. Am. Chem. Soc.* **2017**, *139*, 5309–5312.

[46] Chiba, T.; Hayashi, Y.; Ebe, H.; Hoshi, K.; Sato, J.; Sato, S.; Pu, Y. J.; Ohisa, S.; Kido, J. Anion-exchange red perovskite quantum dots with ammonium iodine salts for highly efficient light-emitting devices. *Nat. Photonics* **2018**, *12*, 681–687.

[47] Paul, S.; Acharya, S. Postsynthesis transformation of halide perovskite nanocrystals. *ACS Energy Lett.* **2022**, *7*, 2136–2155.

[48] Aminzare, M.; Jiang, J.; Mandl, G. A.; Mahshid, S.; Capobianco, J. A.; Dorval Courchesne, N. M. Biomolecules incorporated in halide perovskite nanocrystals: Synthesis, optical properties, and applications. *Nanoscale* **2023**, *15*, 2997–3031.

[49] Chen, D. Z.; Ko, P. K.; Li, C. H. A.; Zou, B. S.; Geng, P.; Guo, L.; Halpert, J. E. Amino acid-passivated pure red $CsPbI_3$ quantum dot LEDs. *ACS Energy Lett.* **2023**, *8*, 410–416.

[50] Shi, J. W.; Li, F. C.; Jin, Y.; Liu, C.; Cohen-Kleinstein, B.; Yuan, S.; Li, Y. Y.; Wang, Z. K.; Yuan, J. Y.; Ma, W. L. *In situ* ligand bonding management of $CsPbI_3$ perovskite quantum dots enables high-performance photovoltaics and red light-emitting diodes. *Angew. Chem., Int. Ed.* **2020**, *59*, 22230–22237.

[51] Song, W. T.; Wang, Y. M.; Wang, B.; Yao, Y. F.; Wang, W. G.; Wu, J. H.; Shen, Q.; Luo, W. J.; Zou, Z. G. Super stable $CsPbBr_3@SiO_2$ tumor imaging reagent by stress-response encapsulation. *Nano Res.* **2020**, *13*, 795–801.

[52] Song, W. T.; Wang, D. D.; Tian, J. W.; Qi, G. B.; Wu, M.; Liu, S. T.; Wang, T. T.; Wang, B.; Yao, Y. F.; Zou, Z. G. et al. Encapsulation of dual-passivated perovskite quantum dots for bio-imaging. *Small* **2022**, *18*, 2204763.

[53] Grandhi, G. K.; Viswanath, N.; S. M.; Cho, H. B.; Kim, S. M.; Im, W. B. Highly stable hetero-structured green-emitting cesium lead bromide nanocrystals via ligand-mediated phase control. *Nanoscale* **2019**, *11*, 21137–21146.

[54] Zhang, Y. H.; Saidaminov, M. I.; Dursun, I.; Yang, H. Z.; Murali, B.; Alarousu, E.; Yengel, E.; Alshankiti, B. A.; Bakr, O. M.; Mohammed, O. F. Zero-dimensional Cs_4PbBr_6 perovskite nanocrystals. *J. Phys. Chem. Lett.* **2017**, *8*, 961–965.

[55] Nikl, M.; Mihokova, E.; Nitsch, K.; Somma, F.; Giampaolo, C.; Pazzi, G. P.; Fabeni, P.; Zazubovich, S. Photoluminescence of Cs_4PbBr_6 crystals and thin films. *Chem. Phys. Lett.* **1999**, *306*, 280–284.

[56] Ren, J. J.; Zhou, X. P.; Wang, Y. H. Water triggered interfacial synthesis of highly luminescent $CsPbX_3$: Mn^{2+} quantum dots from nonluminescent quantum dots. *Nano Res.* **2020**, *13*, 3387–3395.

[57] Yang, D.; Li, P. L.; Zou, Y. T.; Cao, M. H.; Hu, H. C.; Zhong, Q. X.; Hu, J. X.; Sun, B. Q.; Duhm, S.; Xu, Y. et al. Interfacial synthesis of monodisperse $CsPbBr_3$ nanorods with tunable aspect ratio and clean surface for efficient light-emitting diode applications. *Chem. Mater.* **2019**, *31*, 1575–1583.

[58] Huang, H. Y.; Yang, R. T.; Chinn, D.; Munson, C. L. Amine-grafted MCM-48 and silica xerogel as superior sorbents for acidic gas removal from natural gas. *Ind. Eng. Chem. Res.* **2003**, *42*, 2427–2433.

[59] Ravi, V. K.; Santra, P. K.; Joshi, N.; Chugh, J.; Singh, S. K.; Rensmo, H.; Ghosh, P.; Nag, A. Origin of the substitution mechanism for the binding of organic ligands on the surface of $CsPbBr_3$ perovskite nanocubes. *J. Phys. Chem. Lett.* **2017**, *8*, 4988–4994.

[60] Brown, J.; Grimaud, A. Proton-donating and chemistry-dependent buffering capability of amino acids for the hydrogen evolution reaction. *Phys. Chem. Chem. Phys.* **2023**, *25*, 8005–8012.

[61] Liu, M.; Zhao, J. T.; Luo, Z. L.; Sun, Z. H.; Pan, N.; Ding, H. Y.; Wang, X. P. Unveiling solvent-related effect on phase transformations in CsBr–$PbBr_2$ system: Coordination and ratio of precursors. *Chem. Mater.* **2018**, *30*, 5846–5852.

[62] Chen, Y. H.; Smock, S. R.; Flintgruber, A. H.; Perras, F. A.; Brutchey, R. L.; Rossini, A. J. Surface termination of $CsPbBr_3$ perovskite quantum dots determined by solid-state NMR spectroscopy. *J. Am. Chem. Soc.* **2020**, *142*, 6117–6127.